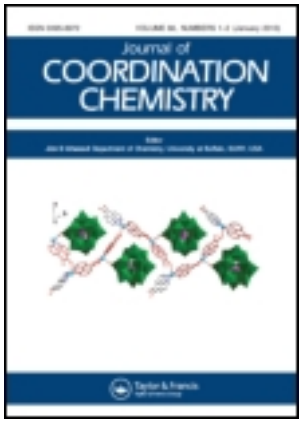

Journal of Coordination Chemistry
Publication details, including instructions for authors and subscription information:
http://www.tandfonline.com/loi/gcoo20

Gas-phase stabilized metal complexes of cyclic peptides - theoretical versus experimental study

Bojidarka Ivanova [a] & Michael Spiteller [a]

[a] Department of Environmental Chemistry and Analytical Chemistry, Faculty of Chemistry, Institute of Environmental Research, Dortmund University , Otto-Hahn-Str. 6, D-44227 Dortmund, Germany

Published online: 04 Apr 2012.

To cite this article: Bojidarka Ivanova & Michael Spiteller (2012) Gas-phase stabilized metal complexes of cyclic peptides - theoretical versus experimental study, Journal of Coordination Chemistry, 65:9, 1548-1568, DOI: 10.1080/00958972.2012.676166

To link to this article: http://dx.doi.org/10.1080/00958972.2012.676166

Journal of Coordination Chemistry
Vol. 65, No. 9, 10 May 2012, 1548–1568

Taylor & Francis
Taylor & Francis Group

Gas-phase stabilized metal complexes of cyclic peptides – theoretical *versus* experimental study

BOJIDARKA IVANOVA* and MICHAEL SPITELLER

Department of Environmental Chemistry and Analytical Chemistry, Faculty of Chemistry, Institute of Environmental Research, Dortmund University, Otto-Hahn-Str. 6, D-44227 Dortmund, Germany

(*Received 13 September 2011; in final form 28 February 2012*)

This article deals with the experimental and theoretical study of the coordination ability and processes of glycyl-penta and hexahomopeptides and corresponding cyclic derivatives with the Ag^{I}, Zn^{II}, and Cu^{II}. Special attention is focused on the observed cyclic small peptide analogues as well as corresponding complexes. These phenomena are studied experimentally by electrospray ionization and matrix-assisted laser desorption ionization mass spectrometric methods. Considering the physical and chemical properties of gas-phase stabilized systems, precisely calculated thermodynamic parameters, physical properties, and structures by the quantum chemical DFT methods are performed. Conformational preferences of the obtained peptide species as well as the complexes are presented. The coordination ability is elucidated in condense phase by electronic absorption, infrared, and Raman spectroscopies, nuclear magnetic resonance, and thermal methods. The Ag^{I}/Ag^{III} redox process observed during the interaction with the peptides is discussed.

Keywords: Cyclic peptides; Metal-organic complexes stable in gas-phase; Mass spectrometry

1. Introduction

Cyclic peptides comprise a large body of natural products (NPs) and synthetic compounds, representing an important class of antibiotics isolated from bacteria, fungi, and plants or prepared synthetically [1]. New derivatives are discovered on a regular basis and have been found to have numerous pharmaceutical applications including their use as enzyme inhibitors, antifungal and antibacterial agents, and immunosuppressant and anticancer drugs [2]. On-going interest in biologically active cyclic peptides has been supported by advanced analytical methods which are needed to characterize the cyclic structures, many of which contain modified amino acids. Characterization of cyclic peptides by mass spectrometry poses a great analytical challenge because they do not have well-defined termini, as do linear peptides, which can be used unambiguously to anchor the assignment of the sequence of amino acids in an orderly fashion. The development of powerful new mass spectrometric techniques such as matrix-assisted laser desorption ionization (MALDI) and electrospray ionization (ESI) has been driven

*Corresponding author. Email: B.Ivanova@infu.tu-dortmund.de; B.Ivanova@web.de

ISSN 0095-8972 print/ISSN 1029-0389 online
http://dx.doi.org/10.1080/00958972.2012.676166

by polymer and biological sciences [3]. Workers in other areas, for whom conventional techniques are less useful, such as inorganic and organometallic chemistry, are now embracing these ionization methods [4]. Anticancer activity of Ag^{I}-coordination compounds has been relatively unexplored until recent studies [5]. Several complexes have shown *in vitro* activity against multiple cell lines. Series of saturated and unsaturated NHC-containing silver(I) chloride complexes were tested against various cell lines and showed higher cytotoxicities than cisplatin [5a].

Our recent studies on NPs [6], including the functional-oriented synthesis of small peptides and their complexes with Ag^{I} [7], have shown that ESI-MS/MS mass spectrometric analysis of the obtained complexes determined the gas-phase stability. For the penta- and hexaglycyl-homopeptides parallel fragmentation processes with the formation of cyclic peptide derivatives have been proposed [8]. Detailed analysis of the nature of these processes are presented in this article, studying the coordination ability of glycyl-homopenta- and hexapeptides with Ag^{I}, Zn^{II}, and Cu^{II} using the ESI-MS/MS and MALDI imaging mass spectrometry (MALDI-MSI), by the Orbitrap analyser. The experimental data are correlated to the results of theoretical quantum chemical analysis of the free ligands, different types of protonated forms, observed molecular fragments, and complexes. This study is of importance for the MALDI-MSI method, due to a relatively large area of application focused on protein and peptide analysis [1–8]. The mass spectrometric and theoretical data are correlated to experimental results from electronic absorption, vibration spectroscopy as well as nuclear magnetic resonance.

2. Experimental

2.1. Physical measurements

X-ray diffraction intensities were measured on a Bruker Smart X2S diffractometer using micro-source Mo-Kα radiation and employing the ω scan mode. The structures in figure 1 are presented by PLATON. An absorption correction was based on multiple-scanned reflections. The crystal structures were solved by direct methods using SHELXS-97 and refined by full-matrix least-squares refinement against F^2. Anisotropic displacement parameters were introduced for all non-hydrogen atoms. Hydrogen atoms attached to carbon were placed at calculated positions and refined allowing them to ride on the parent carbon [9]. HPLC-MS/MS measurements were made using a TSQ 7000 instrument (Thermo Electron Corporation). Two mobile phase compositions were used: (A) 0.1% v/v aqueous HCOOH and (B) 0.1% v/v HCOOH in CH_3CN. For ESI mass spectrometry, a triple quadrupole mass spectrometer (TSQ 7000 Thermo Electron, Dreieich, Germany) equipped with an ESI 2 source was used and operated at the following conditions: capillary temperature 180°C; sheath gas 60 psi, corona 4.5 µA, and spray voltage 4.5 kV. Sample was dissolved in acetonitrile (1 mg mL^{-1}) and was injected in the ion source by an autosampler (Surveyor) with a flow of pure acetonitrile (0.2 mL min^{-1}). Data processing was performed by Excalibur 1.4 software. A standard LTQ Orbitrap XL instrument is used for all experimental work described in this article. An overall mass range of m/z 100–1000 is scanned simultaneously in the Orbitrap analyzer. The samples are measured in solid state, using a variant of the spray technique of solution, containing the matrix and analyte compound. The solution of thus

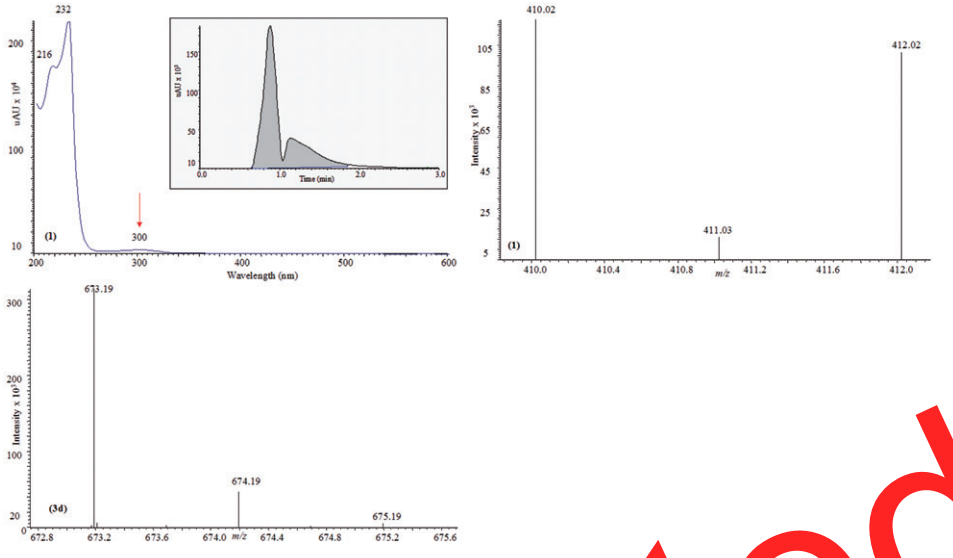

Figure 1. ESI-MS and ESI-MS/MS spectra; electronic transition and mass chromatogram.

obtained thin liquid films is rapidly evaporated to form the sample of matrix/matrix/analyte. The content of metal ions are obtained by ICP measurements on the ICP–OES Thermo Elemental spectrometer with atomisator: Argon–plasma; detection is done by the following lines for Zn (202.5, 206.2, and 213.8 nm) and for Ag (328.0 and 338.2 nm), respectively. UV-Vis-NIR spectra between 190 and 1190 nm using acetonitrile (Uvasol, Merck product) at 2.5×10^{-5} mol L^{-1} in 0.921 cm quartz cells were recorded on a Tecan Safire Absorbance/Fluorescence XFluor 4 V 4.40 spectrophotometer. Conventional IR and Raman spectroscopy in solid-state were performed on a Thermo Nicolet 6700 FTIR spectrometer (4000–400 cm^{-1}, resolution 0.5 cm^{-1}, and 100 scans) and an NXR FT-Raman module within the 4000–50 cm^{-1} region. The thermogravimetric study was carried out using a Perkin-Elmer TGS2 instrument. Calorimetric measurements were performed on a DSC-2C Perkin Elmer apparatus under argon. The ^{1}H- and ^{13}C-NMR measurements were performed at 298 K with a Bruker DRX-600 spectrometer using 5 mm tubes and D_2O as solvent. The chemical shift reference was sodium 3-(trimethylsilyl)tetradeuteriopropionate.

2.2. *Synthesis*

The Ag^{I}, Zn^{II}, and Cu^{II} complexes of the penta- **1–3** and hexa- **1a–3a** glycylhomopeptides were obtained according to a common procedure: equimolar aqueous solutions of the ligands (Bachem Organics) were mixed with corresponding metal salts $CuCl_2 \cdot 2H_2O$ (Merck, 0.1705 g), $AgNO_3$ (Merck, 0.1698 g), and $ZnCl_2$ (Sigma, 0.1367 g). Thus obtained solutions are continuously stirred with heating at 40°C for up to 10 h. The pH values are kept in the range 3.1–4.0 by the dropwise addition of 1×10^{-4} mol L^{-1} water solution of NaOH. In the case of Ag(I) complexes when pH values are 6.0–8.0 metal ion is reduced to Ag(0). Precipitates from the newly synthesized complexes, used as matrices

Table 1. Crystallographic and refinement data for **1**.

Empirical formula	$AgC_{10}H_{14}N_5O_6$
Formula weight	407.20
Temperature (K)	198(2)
Wavelength (Å)	0.71073
Crystal system	Triclinic
Space group	$P\bar{1}$
Unit cell dimensions (Å, °)	
a	8.891(3)
b	10.254(2)
c	23.652(6)
α	90.336(6)
β	100.093(8)
γ	96.228(5)
Volume (Å^3), Z	1032.7(2), 2
Calculated density (Mg m^{-3})	1.564
Absorption coefficient (mm^{-1})	2.731
Crystal size (mm^3)	$0.01 \times 0.04 \times 0.08$
Goodness-of-fit on F^2	2.371
R_1 [$I > 2\sigma(I)$]	0.3269

for the mass spectrometric measurements, are obtained after a week. All of them are filtered off, washed with water, and dried in air at room temperature. The Zn^{II} and Cu^{II} complexes are stable in ambient conditions for more than 2.0 months, while the Ag^{I}-complex turns to a black precipitate (reduction of Ag(I) to Ag(0)) after a month. The yield of the precipitates is 45–62%. Elemental Anal.: (**1**): Found (%): C, 29.10; H, 3.48; N, 17.10; [$Ag^{I}C_{10}H_{14}N_5O_6$] Calcd (%): C, 29.43; H, 3.46; N, 17.16; (**2**): Found (%): C, 31.77; H, 3.83; N, 19.10; [$Zn^{II}C_{10}H_{14}N_5O_6$]; Calcd (%): C, 32.85; H, 3.86; N, 19.18; (**3**): Found (%): C, 33.71; H, 3.54; N, 19.35; [$Cu^{II}C_{10}H_{14}N_5O_6$]; Calcd (%): C, 33.02; H, 3.88; N, 19.25; (**1a**): Found (%): C, 26.05; H, 3.00; N, 15.17; [$Ag^{I}C_{12}H_{17}N_6O_7$]; Calcd (%): C, 34.24; H, 4.07; N, 19.97; (**2a**): Found (%): C, 35.11; H, 3.01; N, 19.68; [$Zn^{II}C_{12}H_{17}N_6O_7$]; Calcd (%): C, 34.10; H, 4.05; N, 19.88; and (**3a**): Found (%): C, 34.50; H, 4.55; N, 19.79; [$Cu^{II}C_{12}H_{17}N_6O_7$]; Calcd (%): C, 34.24; H, 4.07; N, 19.97. Re-crystallization of **1** from methanol : water 1 : 1 resulted in the formation of thin 1-D crystals. The low single-crystal quality, due to the presence of the air bubbles, resulted in the obtained crystallographically high R_1 factor of 33% (table 1, figure 2).

2.3. *Computational methods [10]*

Quantum chemical calculations are performed with Gaussian 98, 09 [10a], and Dalton 2.0 [10b] program packages. The output files were visualized by GaussView03 program package [10c]. The geometries of the studied species were optimized by density functional theory (DFT), employing B3LYP, B3PW91, and M06-2X functionals [10d–h]. Molecular geometries of the studied species were fully optimized by the force gradient method using Bernys' algorithm. For every structure the stationary points found on the molecule potential energy hypersurfaces were characterized using standard analytical harmonic vibrational analysis. The absence of imaginary frequencies, as well as of negative eigenvalues of the second-derivative matrix, confirmed that the stationary points correspond to minima of the potential energy hypersurfaces. Description of the theoretical methods exists for organic species [10i–n] and metal

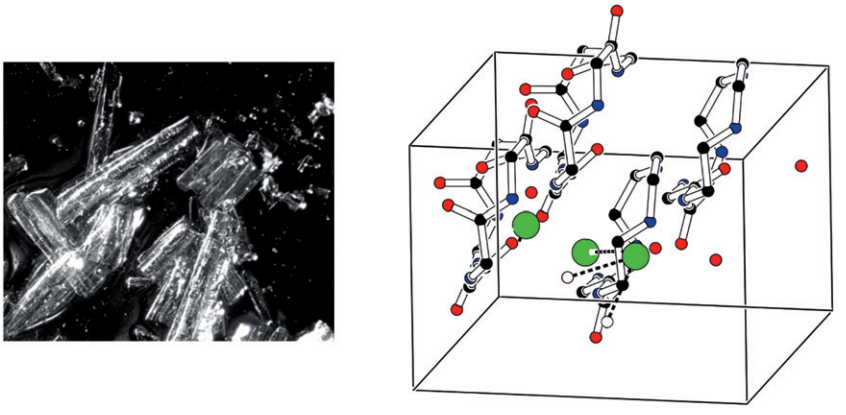

Figure 2. Photographs of the crystals of **1**; PLATON diagram of the unit cell content for **1**; hydrogen atoms are omitted.

complexes [10o–q]. Geometry of the neutral species are optimized and preoptimized at higher levels, using the B3LYP functional at large correlation basis sets such as aug-cc-pVDZ and aug-cc-pVTZ (augmented correlation-consistent polarized valence double and triple zeta levels). For the charged metal complexes the corresponding geometry optimization was performed using B3PW91, utilizing the triple-ζ quality TZVP, triple-ζ plus double polarization TZ2P, Los Alamos National Laboratory's 2 double-ζ as well as quasirelativistic effective core pseudopotentials from Stuttgart–Dresden (LANL2DZ or SDD) [10r, s]. The minimized energies and calculations of the initial force constants were performed using the corresponding net charges and spin multiplicity 2 as well as unrestricted open shell wave function, independent of the used quantum chemical packages. Electronic properties and transitions of the geometrically optimized species were obtained by the M06-2X functional (Gaussian 09 or Dalton 2.0) at aug-cc-pVDZ basis set for peptides and LANL2DZ or SDD for complexes. Calculations by Dalton 2.0 were performed using the GaussianPluging and corresponding in-/output sub-programs for extra functional and basis sets [10t–w]. Calculation of vibrational frequencies and infrared intensities were checked to establish which kind of performed calculations agree best with the experimental data. The electronic absorption and fluorescence spectra in the gas phase and methanol are by TDDFT calculations at above levels of theory. We have utilized primarily the polarizable continuum model (PCM) for calculations of electronic spectra, using the different dielectric constant values and number of points per sphere, respectively, under the above mentioned computational details. The calculated q_N(NBO) charges for the peptides and metal complexes were obtained using the natural bond orbital analysis (NBO) at same computational inputs.

2.4. *Statistical and mathematical methods [11]*

The experimental and theoretical spectroscopic patterns were processed by R4Cal OpenOffice STATISTICs for Windows 7 program package [11a]. Baseline corrections and curve-fitting procedures were applied. The baseline was calculated using the

standard linear equation. Non-linear peak fitting methods are applied, involving a fitting of series of individual functions simultaneously, in order to obtain the single "best fit" solution. Solutions were found by iteratively trying a series of combinations of parameters until the best is found. Since the solutions are interdependent, small changes in one of the parameters affect the final result of all the others. When using an iterative process, the starting point should be as close to the actual solution as possible. Good "guestimates" for the starting values increase the probability of finding the "best" solution [11b, c]. Using non-linear methods requires a threshold at which the "fit" is considered "good" [11d–f]. In the case of the Levenberg–Marquardt method, the merit equation used is the χ^2 equation [11d–g]. The final solution is found when a minimum in the reduced χ^2 equation is reached. It is a statistical measure of "goodness-of-fit," inversely proportional to the known variance of the data set. The statistical significance of each regression coefficient was checked by the use of *t*-test (calculation of the significance using data from the experimental error, usually higher than 0.100). The model fit was determined by *F*-test (comparison of calculated and experimentally obtained signal values) [11b, c].

3. Results and discussion

3.1. *ESI-MS/MS spectra of H-(Gly)$_5$-OH and H-(Gly)$_6$-OH and their complexes*

ESI-MS data of positive, both in single (*MS*) and tandem (*MS*/*MS*) mode yield molecular weights of the small peptides and their complexes together with structural information [12]. It is the method of choice for the analysis of small peptides and their metal complexes, as a result of the high sensitivity and selectivity of the method [1–8, 12]. Moreover, the isotope patterns of the metal ions facilitate identification of the corresponding complexes in the gas phase [4a]. As shown in our previous papers [7g, h], the homo penta- and hexapeptides are characterized with the peaks at *m*/*z* 304.13 and 361.15, corresponding to singly charged cations $[C_{10}H_{18}NO_6N_5]^+$ and $[C_{12}H_{21}O_7N_6]^+$ with the molecular weight of 304.28 and 361.63, respectively. A peak at *m*/*z* 607.25 in the first case is observed in the ESI-MS spectrum and probably corresponds to the dimeric associate (non-covalent bonded peptides) [13]. According to our studies on humic and fulvic acids, where preferred ionization in the positive mode for the amines is observed [12], it would be expected that the NH_3^+ derivatives of the peptides would be formed in the gas phase as well as a stable $NH_3^+\cdots O(H)CO$ bond. Our calculations of the Gibbs free energies show a ΔG of –278.12 kcal mol^{-1}, assuming a stable gas-phase species of peptide dimers. Fragmentation of the peptides yields a series of cyclic derivatives [8], which are found in corresponding mass spectra of H-(*Gly*)$_5$-OH and H-(*Gly*)$_6$-OH (figure 1). The observed series with peaks at *m*/*z* 286.11 ($[C_{10}H_{16}O_5N_5]^+$), 229.09 ($[C_8H_{13}O_4N_4]^+$), and 190.08 ($[C_6H_{10}O_3N_3]^+$) correspond to cyclic penta-, tetra-, and tripeptides. The ESI-MS spectrum of hexapeptide is characterized in addition with the peak at 343.13, belonging to the cyclic hexapeptide. The ΔG value of the cyclic hexapeptide is characterized with the lowest value (table 2). In the ESI-MS spectrum of (**1a**) [6h], peaks at *m*/*z* 467.03/469.03 correspond to Ag^{III}-complex of glycyl hexapeptide $[^{107}Ag^{III}C_{12}H_{20}O_7N_6]^+/[^{109}Ag^{III}C_{12}H_{20}O_7N_6]^+$. The corresponding data for **1** have peaks at *m*/*z* 410.02/412.02 of $[^{107}Ag^{III}C_{10}H_{18}O_6N_5]^+/[^{109}Ag^{III}C_{10}H_{18}O_6N_5]^+$ (figure 1).

Table 2. Theoretical (B3PW91/LANL2DZ and B3PW91/SDD gas-phase, and solution) values of the atomic charges, natural electron configuration (NEC), and total energy of the given studied species with pre-optimization of the geometry. The calculations in polar medium are performed using the PCM model.

	Charges		NEC		E_{tot} (kcal mol^{-1}) (without solvent energy)
	Gas-phase	Polar	Gas-phase	Polar	Polar
$Zn^{II}(H_2O)_4(NH_3)_2$					-198.1_4
Zn	1.7459_3	−27.4622	…4s(0.26)3d(**9.97**)	…4s(0.26)3d(**9.97**)	
N	−1.2343	−1.2411	…2s(1.51)2p(4.70)	…2s(1.51)2p(4.72)	
N	−1.2257	−1.2322	…2s(1.51)2p(4.71)	…2s(1.51)2p(4.72)	
O	−0.9587	−0.9807	…2s(1.72)2p(5.23)	…2s(1.72)2p(5.25)	
O	−1.0281	−1.0431	…2s(1.74)2p(5.28)	…2s(1.74)2p(5.29)	
O	−1.0371	−1.0375	…2s(1.74)2p(5.29)	…2s(1.74)2p(5.30)	
O	−1.0264	−1.0434	…2s(1.72)2p(5.23)	…2s(1.74)2p(5.30)	
$Zn^{II}(H_2O)(NH_3)_3Cl$					-81.5_1
Zn	1.6526_8	−26.7579	…4s(0.34)3d(**9.97**)	…4s(0.32)3d(**9.97**)	
N	−1.2427	−1.2661	…2s(1.53)2p(4.69)	…2s(1.53)2p(4.72)	
N	−1.1999	−1.2327	…2s(1.52)2p(4.67)	…2s(1.52)2p(4.70)	
N	−1.2209	−1.2325	…2s(1.52)2p(4.68)	…2s(1.52)2p(4.70)	
O	−1.0287	−1.0446	…2s(1.74)2p(5.28)	…2s(1.74)2p(5.28)	
Cl	−0.7977	−0.8528	…3s(1.97)3p(5.83)	…3s(1.98)3p(5.88)	
$Ag^{III}(NH_3)_4$					**-467.9_1**
Ag	1.4674_2	-35.9029_1	…5s(0.44)4d(**9.16**)	…5s(0.43)4d(**9.16**)	
N	−1.13707	−1.14075	…2s(1.53)2p(4.60)	…2s(1.52)2p(4.61)	
N	−1.05353	−1.06566	…2s(1.45)2p(4.59)	…2s(1.45)2p(4.59)	
N	−1.10441	−1.10834	…2s(1.52)2p(4.57)	…2s(1.52)2p(4.57)	
N	−0.85755	−0.85423	…2s(1.41)2p(4.42)	…2s(1.41)2p(4.41)	
$Ag^{III}(OH_2)_4$					**−536.19**
Ag	1.6176_5	-35.8407_2	…6s(0.41)4d(**9.82**)	…6s(0.41)4d(**9.10**)	
O	−0.5535	−0.9287	…2s(1.50)2p(5.03)	…2s(1.73)2p(5.20)	
O	−0.8528	−0.6347	…2s(1.64)2p(5.19)	…2s(1.64)2p(4.95)	
O	−0.8188	−0.5671	…2s(1.77)2p(5.04)	…2s(1.77)2p(5.04)	
O	−0.5533	−0.5441	…2s(1.68)2p(4.84)	…2s(1.66)2p(4.86)	
$Ag^{III}(NH_3)_2(OH_2)_2$					**−517.00**
Ag	1.5721_5	-35.8864_1	…6s(0.35)4d(**9.16**)	…6s(0.35)4d(**9.16**)	
N	−1.0727	−1.0903	…2s(1.43)2p(4.32)	…2s(1.43)2p(4.32)	
N	−0.7791	−0.7734	…2s(1.46)2p(4.59)	…2s(1.46)2p(4.61)	
O	−0.5628	−0.8877	…2s(1.77)2p(5.04)	…2s(1.77)2p(5.11)	
O	−0.8204	−0.5998	…2s(1.49)2p(5.04)	…2s(1.49)2p(5.08)	
$Ag^{III}(NH_3)_4$					−468.31
Ag	1.6207_1	-67.9087_5	…6s(0.53)5d(**8.92**)	…6s(0.52)5d(**8.92**)	
N	−1.1204	−1.1241	…2s(1.53)2p(4.59)	…2s(1.45)2p(4.63)	
N	−1.0940	−1.1053	…2s(1.45)2p(4.62)	…2s(1.53)2p(4.59)	
N	−1.0900	−1.0926	…2s(1.52)2p(4.55)	…2s(1.52)2p(4.56)	
N	−0.8727	−0.8708	…2s(1.41)2p(4.44)	…2s(1.41)2p(4.43)	

Zn^{II} and Cu^{II} also show stable gas-phase complexes with the linear peptides, with signals at *m*/*z* 424.27/426.27 ($[^{63}Cu^{II}C_{12}H_{20}O_7N_6]^+/[^{65}Cu^{II}C_{12}H_{20}O_7N_6]^+$ (**3a**)), 362.20/364.20/366.20 ($[^{64}Zn^{II}C_{10}H_{18}O_6N_5]^+/[^{66}Zn^{II}C_{10}H_{18}O_6N_5]^+/[^{68}Zn^{II}C_{10}H_{18}O_6N_5]^+$ (**2**)), 424.15/426.15/468.15 ($[^{64}Zn^{II}C_{12}H_{20}O_7N_6]^+/[^{66}Zn^{II}C_{12}H_{20}O_7N_6]^+/[^{68}Zn^{II}C_{12}H_{20}O_7N_6]^+$ (**2a**)), 365.18/367.18 ($[^{63}Cu^{II}C_{10}H_{18}O_6N_5]^+/[^{65}Cu^{II}C_{10}H_{18}O_6N_5]^+$ (**3**)). The obtained data are in accord with the isotope ratio distribution of the corresponding metal ions of $^{107/109}$Ag (51.81/48.11%), $^{64/66/68}$Zn (48.89/27.81/18.52%), and $^{63/65}$Cu (69.09/30.91%), and the

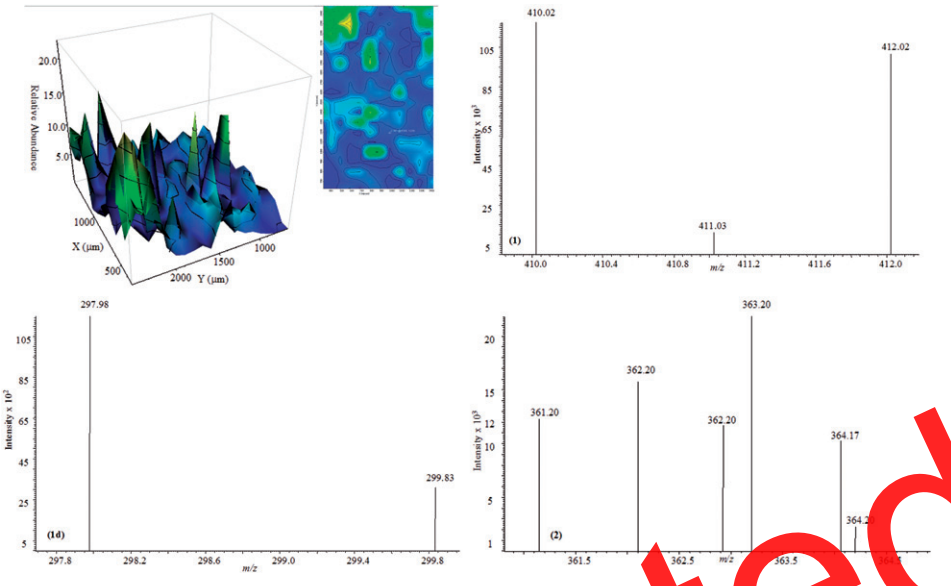

Figure 3. 3-D and 2-D images by logarithm plotting of Δx, Δy *vs.* the signal amplitude (grid) of selected ion range as a function of the location of the surface of **1**; The MALDI-IMS of **1b**, **1d**, and **2**, respectively.

calculated mass spectrometric intensity ratios show quantitative amounts of each of the complex species [4a]. The peaks of the cyclic peptides are present in mass spectra of the free ligands. Corresponding data for the complexes with the cyclic peptides show peaks at *m/z* 391.99/393.99 ($[^{107}Ag^{III}C_{10}H_{16}O_5N_5]^+/[^{109}Ag^{III}C_{10}H_{16}O_5N_5]^+$ (**1b**)), 248.09/250.09/252.09 ($[^{64}Zn^{II}C_{10}H_{16}O_5N_5]^+/[^{66}Zn^{II}C_{10}H_{16}O_5N_5]^+/^{68}Zn^{II}C_{10}H_{16}O_5N_5]^+$ (**2b**)), 251.96/253.96 ($[^{63}Cu^{II}C_{10}H_{16}O_5N_5]^+/[^{65}Cu^{II}C_{10}H_{16}O_5N_5]^+$ (**3b**)), 336.86/338.86 ($[^{107}Ag^{III}C_8H_{16}O_4N_4]^+/[^{109}Ag^{III}C_8H_{16}O_4N_4]^+$ (**1c**)), 292.09/294.09/296.09 ($[^{64}Zn^{II}C_8H_{16}O_4N_4]^+/[^{66}Zn^{II}C_8H_{16}O_4N_4]^+/^{68}Zn^{II}C_8H_{16}O_4N_4]^+$ (**2c**)), 294.99/296.99 ($[^{63}Cu^{II}C_8H_{16}O_4N_4]^+/[^{65}Cu^{II}C_8H_{16}O_4N_4]^+$ (**3c**)), respectively (figures 1 and 3). With the cyclic tripeptide only an Ag^{III}-complex is found (peaks at *m/z* 297.98/299.98, ($[^{107}Ag^{III}C_6H_{10}O_3N_3]^+/[^{109}Ag^{III}C_6H_{10}O_3N_3]^+$ (**1d**)). A Cu^{II}-complex (**3d**) of the dimer of the glycyl-homopentapeptide is also found in the gas phase (peaks at 673.19/675.19), figure 1. Since the corresponding ligands are present in the linear form, we could expect bidentate coordination of the metal ion through the $N_{(termini)}$ at molar ratio metal to ligand 1 : 2. Our results could correlate with the ion radius of the metal. In all cases the mass spectrometric conditions result in the stabilization of Ag^{III}-complexes of the peptides. In contrast to the linear peptides, where tetradentate coordination of the metal ions is expected by $N_{(termini)}$ of the ligands, the gas-phase complexes with cyclic analogues are through the O-amide centers, also tetradentate. The theoretical ΔG values support strongly the assumed coordination, thus giving differences within (−56.12) to (−68.13) kcal mol^{-1} (table 2). The obtained result agrees with the known Ag^I complexes with the naturally obtained cyclic peptides, with coordination to the macrocycle carbonyl groups [1a–c]. Further studies on the coordination of natural cyclic derivatives with the larger ring size, allowing tuning of the coordination of peptide systems, depending on the reaction conditions are needed.

3.2. *MALDI-MSI spectra of H-(Gly)$_5$-OH and H-(Gly)$_6$-OH and their complexes*

The softer conditions in ESI allow observing the peak for non-covalent interacting dimers of peptides in the gas-phase. In contrast, MALDI-MSI spectra show the peaks only of the free linear and cyclic peptides (figure 3). Experiments with molar ratios metal-to-ligand 4 : 1–6 : 1 are in accord with the ESI data and allow observation of peaks of the metal-organic species, since the corresponding ones of the free ligands are negligible. For cyclic peptides we could describe the systems in analogy with the coordination chemistry of crown ethers with selectivity of the ligands towards the metal ions allowing their quantitative detection by MALDI-MSI. On this basis, tuning of the coordination ability of cyclic functionalized peptides could be used for selective detection of metal ions. Assignment of all peaks obtained by defragmentation of the cyclic peptides and their metal complexes as well as the molecular fragments of the corresponding linear analogues is complicated. Determination of amino-acid sequences of cyclic peptides by one stage of mass spectrometry was compromised by multiple and indiscriminate ring-opening pathways, resulting in a set of acylium ions of the same m/z. Moreover, in the case of glycyl homopeptides the equal probability of ring opening exists for all gly$_1$–gly$_5$(gly$_6$) residues. These ions fragment, giving spectra that are superpositions of spectra from fragmentation of the various ring-opened forms [8a, b]. Dissociation patterns of metal complexes of linear peptides, as alternative of protonation for structural characterization of peptides, show that the metal cation may bind at the C$_{(termini)}$, N$_{(termini)}$, or at an interior residue depending on the metal ion and the peptide sequence. Fragmentation tended to be much more specific for the metal complexes, with the metal ion directing cleavage at a certain residue or terminus (figures 1 and 3). The obtained data are also in accord with model systems $Zn^{II}(OH_2)_4(NH_3)_2$ and $Zn(H_2O)(NH_3)_3Cl$ of distorted O_h symmetry, $Zn^{II}O_6$ unit, already discussed [4h] as well as perturbed square pyramidal geometry (table 2). Theoretical NBO analysis unambiguously prove perturbed T_d chromophores for Ag^I complexes [7f–i].

3.3. *Electronic absorption spectra*

Experimentally obtained UV-Vis spectra of **1** and **2** are characterized with absorption bands at 300–350 nm and ε_ν within 2023–3410 L mol^{-1} cm^{-1}. Assignment of the experimental results, especially for broad overlapped patterns such as these, application of the mathematical methods for their interpretation and corresponding statistical tools for the evaluation of best fit are important. The data (figure 4) used curve-fitting procedure and non-linear methods for approximation. Application of these methods, especially for overlapped curves, as shown in band sub-components in black and grey shaded areas, could lead to obtaining artifacts (e.g., the sub-maximum at 275 nm) or could effect the absolute quantity of the defined λ_{max} and ε_ν values. This is also valid when spectra have low signal-to-noise values (S/N) (see, e.g., the black shaded area in figure 5). In all mathematical procedures for interpretation of the experimentally obtained spectroscopic patterns (figure 4, inset), a preliminary baseline correction is performed. The observed maxima are assigned as charge transfer (CT) bands, which correlate well with the obtained ε values. In our case the band is bathochromic shifted more than 50 nm due to the participation of more than two deprotonated amide and primary amino groups in tetradentate chelation. The CT bands of Ag^I and Zn^{II} have

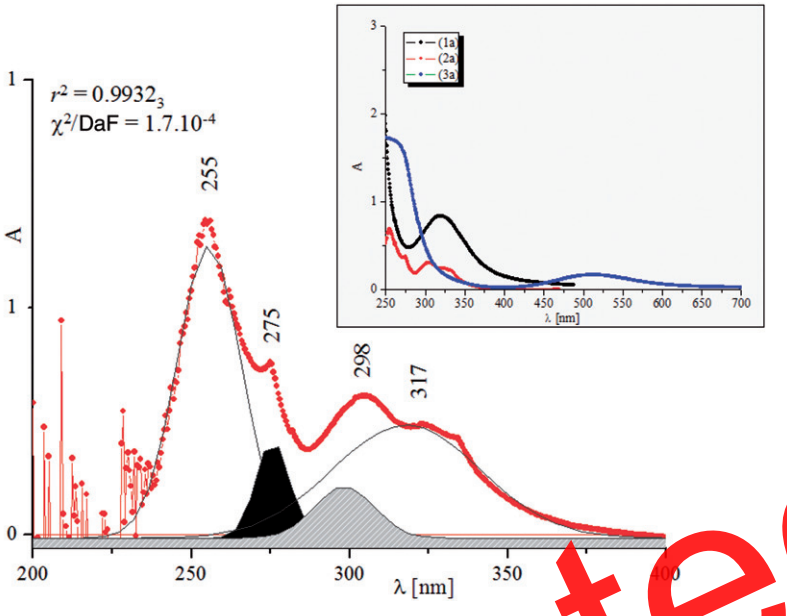

Figure 4. Mathematical procedure spectroscopic pattern with baseline correction and non-linear curve-fitting using the Gaussian function; The r^2 refers to (χ^2/DaF) statistical values of the experimental spectroscopic pattern of the electronic absorption spectrum of **2a**; The obtained relatively low r^2 value in is associated with the low S/N ratio within the 200–250 nm region (see ref. [16]). Inset: Experimental electronic absorption spectra of **1a–3a** in methanol at 2.4×10^{-4} mol L^{-1} concentration without the applied mathematical procedure. The experimental spectroscopic curve are presented by dotted-lines.

decreasing intensity about 20% in comparison with the corresponding Pt^{II} complex and an additional bathochromic shift of *ca* 25 nm. The CT for the metal complexes with completed d-shells such as Zn^{II} and Ag^{I} need further discussion. Similar to the other complexes of d^{10} and d^8 metal ions a metal-to-ligand charge-transfer (MLCT) (figure 1) [7g, h] as well as metal-to-ligand one [7i], result in the observed optical phenomena both in condensed and gas-phase. In our cases the obtained data agree well with the mass spectrometric results discussed above. The parallel study of the corresponding Cu^{II} complex of both peptides, where electronic absorption spectra unambiguously define tetradentate coordination of the metal through $N_{(termini)}$ (scheme 1) [14] show a significant CT effect as expected for Cu^{II}-complexes. The ε_ν of 5723 L mol^{-1} cm^{-1} is found at $\lambda_{max} = 314$ nm; bands at 500–550 nm are classical d → d transitions ($\varepsilon_\nu = 97$ L mol^{-1} cm^{-1}). In this case the Jahn–Teller effect stabilizes the metal complex for d^9, by analogy with d^8 metal complexes [6i]. The spectroscopic profile with d^{10} metal ions illustrates the CT effect as dominant, as well as associated with the gas-phase stabilization of the corresponding complexes.

3.4. *Vibrational (IR- and Raman) data*

Tetradentate coordination of *H-(Gly)$_5$-OH* and *H-(Gly)$_6$-OH* through $N_{(termini)}$, scheme 1, by the deprotonated ligands and with protonation of the COOH-group is proposed from IR- and Raman spectra (figure 5). In all the complexes disappearance of

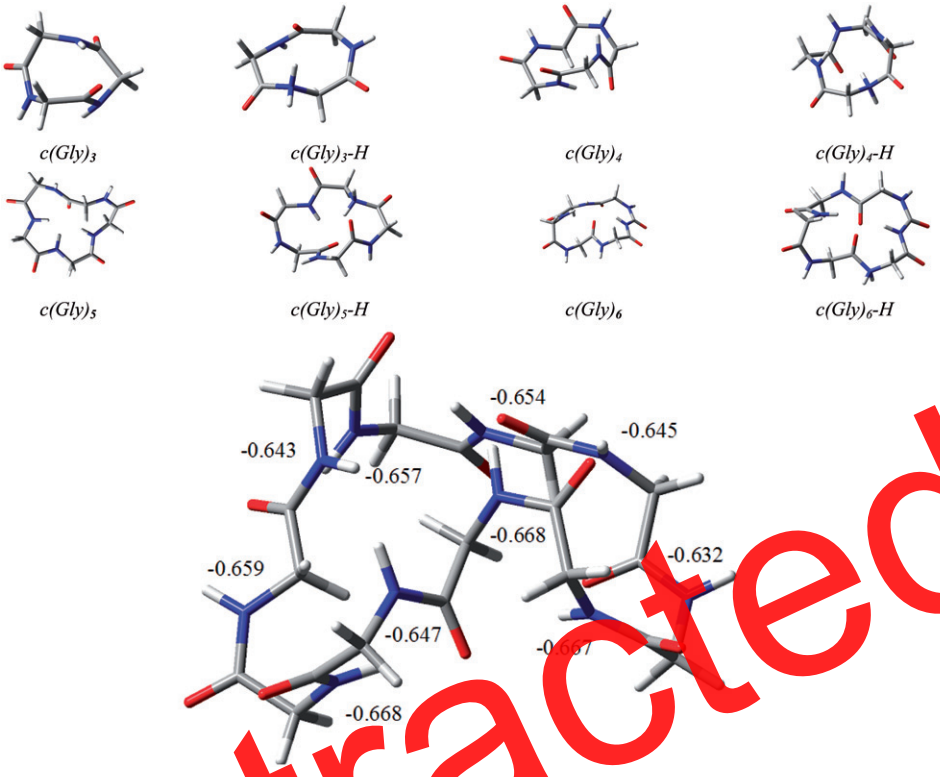

Scheme 1. Most stable conformers of the neutral cyclic peptides and their protonated forms; The *H*-$(Gly)_n$-*OH* and *H*-$(Gly)_n$-*COOH* ($n = 5$ or 6) are the corresponding zwitterion and protonated forms of the peptides; The *c*$(Gly)_n$ and *c*$(Gly)_n$-*H*, where $n = 3$–6, are the cyclic derivatives, respectively; The q_N(NBO) values of the cyclic dimer of glycyl homo pentapeptide.

amide ν_{NH} and δ_{NH} as well as high-frequency shift of three of the amide I peaks is observed. Bands from 1750 to 1735 cm^{-1} are associated with $\nu_{C=O}$ of the reversed COOH-group. When the oxygen of COO^- is coordinated the observed maximum is shifted to lower frequency, about 20 cm^{-1} [7]. The absence of characteristic NH_3^+ bands in the ligands and observation of (ν^{as}_{NH2} and ν^{as}_{NH2}) and (δ_{NH2}) for NH_2 with values typical for coordinated primary NH_2 supports $N_{(amino)}$ in coordination. The low-intensity bands of the NH_3^+ fragment in the free peptides in Raman spectra allow evaluation of the coordination ability by the intense Amide I frequencies at 1700–1550 cm^{-1}. Similar to electronic transitions, the IR- and Raman data (figure 5) were evaluated, applying mixed non-linear Gaussian–Lorenzian function (experimental). Precise assignment of the absolute values of peak positions and the integral intensities could be affected by several factors. As shown in figure 5, the low S/N value for 1660–1620 cm^{-1} leads to perturbation of the absolute quantity of the peak at 1645 cm^{-1}. Thus, the values should be carefully interpreted, especially for coordination ability. Since frequency shifts of the bands when compared to free ligands, in the cases of the complex and complicated curves, the obtained data should be confirmed by other independent physical methods. The corresponding IR-data for isolated Ag^I-, Zn^{II}-, and Cu^{II}-complexes are summarized in table 3.

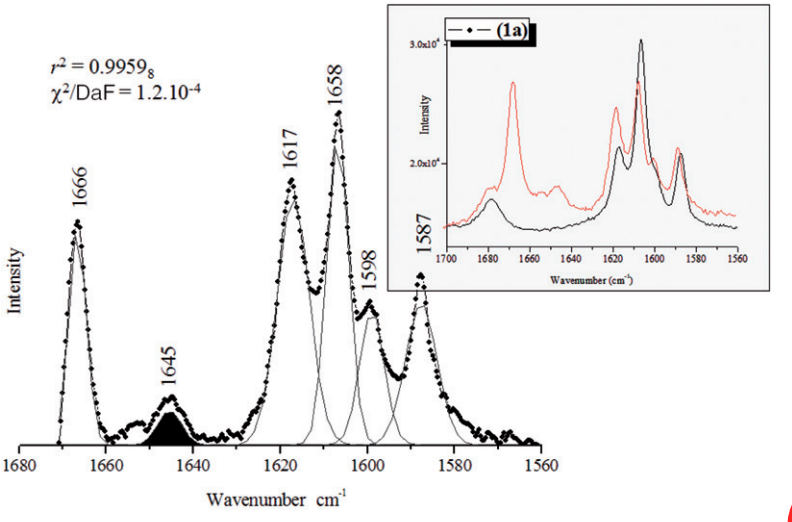

Figure 5. Mathematical procedure for solid-state Raman spectrum of **1a** with baseline correction method and non-linear curve-fitting using the Gaussian to Lorenzian mixed function; The r^2 refers to (χ^2/DaF) statistical values. Small figure: Experimental non-mathematical procedure for solid-state Raman spectra of *H-(Gly)$_6$-OH* (black line) and the corresponding metal complex (**1a**) from 1700 to 1550 cm^{-1} (gray line).

For isolated metal complexes, observation of the new low-intensity frequencies from 440–360 cm^{-1} (Ag^{I}-complexes), 440–338 cm^{-1} (Zn^{II}-complexes), and 400 cm^{-1} (Cu^{II}-complexes), respectively (figure 6), are characteristic for ν_{M-N} stretches [7h]. Their low-intensity and the relatively low S/N ratio makes determination of the absolute values difficult (figure 6). The vibrations are typical for the studied metal ions with other O- and N-containing ligands [15]. The observed excitations at 200–30 cm^{-1} are assigned to H-bond deformations (120–100 cm^{-1}), skeletal, and coupling modes (100–60 cm^{-1}) as well as torsions of side chains (50–30 cm^{-1}), respectively.

3.5. *Nuclear-magnetic resonance data*

In contrast to coordination for smaller glycyl-containing homopeptides [7], the ^{1}H-NMR chemical shifts for penta- and hexa-derivatives show significant differences for **C**H$_2$ protons at the N$_{(termini)}$ (3.45–3.89 ppm, gly$_1$–gly$_4$). The chemical shift differences $\Delta\delta$ are +0.51 ppm. The ^{13}C-NMR data agree well with this assumption as far as the CH$_2$ N$_{(termini)}$ carbon chemical shifts are at 41.60 ppm, upfield with $\Delta\delta$ *ca* −0.92 ppm. Protonation of **C**OO$^-$ in the zwitterion peptides after coordination with the metal ions weakly affects the signal, downfield shift to 174.00 ppm ($\Delta\delta$ within 4.11–4.23 ppm). This result supports only the N$_{(termini)}$ of the peptides taking part in coordination. The $\Delta\delta$ values *ca* 12.00 ppm are found when the peptides coordinate through the C$_{(termini)}$ as well. Molecular flexibility and the large number of possible conformations allow conformational analysis only in the case of unequivocal assignments of resonances. In cyclic derivatives the data were characteristic of one stable conformer [16], exhibiting stability due to the presence of intramolecular NH···O=C hydrogen bonds (scheme 1). The high-field NH resonance at 5.7 ppm was

Table 3. IR-spectroscopic data in solid-state of the obtained metal-organic Ag^{I}, Zn^{II}, and Cu^{II}-complexes with the peptides.

	ν [cm^{-1}]							
Assignment	H-(Gly)$_5$-OH [7h]	**1**	**2**	**3**	H-(Gly)$_6$-OH [7h]	**1a**	**2a**	**3a**
ν^{as}_{NH2}, ν^{s}_{NH2}	–	3392, 3218	3412, 3227	3452, 3208	–	3398, 3205	3411, 3217	3405, 3208
ν_{NH}	3302, 3298, 3284, 3269	3300	3263	3307	3332, 3327, 3310, 3300, 3275	3365, 3202	3377, 3209	3391, 3405
ν^{as}_{NH3+}, ν^{s}_{NH3+}	3100–2500	–	–	–	3200–2400	–	–	–
$\nu_{C=O(COOH)}$	–	1737	1742	1744	–	1728	1739	1742
δ^{as}_{NH3+}	1698, 1688	–	–	–	1690, 1689	–	–	–
$\nu_{C=O\ (Amide\ I)}$	1684, 1674, 1659, 1632	1681, 1675, 1652, 1631	1681, 1677, 1655, 1630	1683, 1670, 1651, 1638	1686, 1676, 1660, 1635, 1627	1686, 1677, 1658, 1630, 1622	1682, 1670, 1667, 1631, 1625	1682, 1670, 1668, 1631, 1625
ν^{as}_{COO-}	1563	–	–	–	1560	–	–	–
$\delta_{NH\ (Amide\ II)}$	1578, 1568, 1561, 1541	1550	1558	1555	1548, 1537, 1524, 1513, 1502	1544, 1558	1550, 1560	1552, 1559
δ^{S}_{NH3+}	1529	–	–	–	1527	–	–	–
ν^{S}_{COO-}	1413	–			1405	–		
$\gamma_{NH\ (Amide\ V)}$	727, 722, 713, 700	746	782	700	727, 720, 692, 694, 672	730, 742	727, 769	736, 760

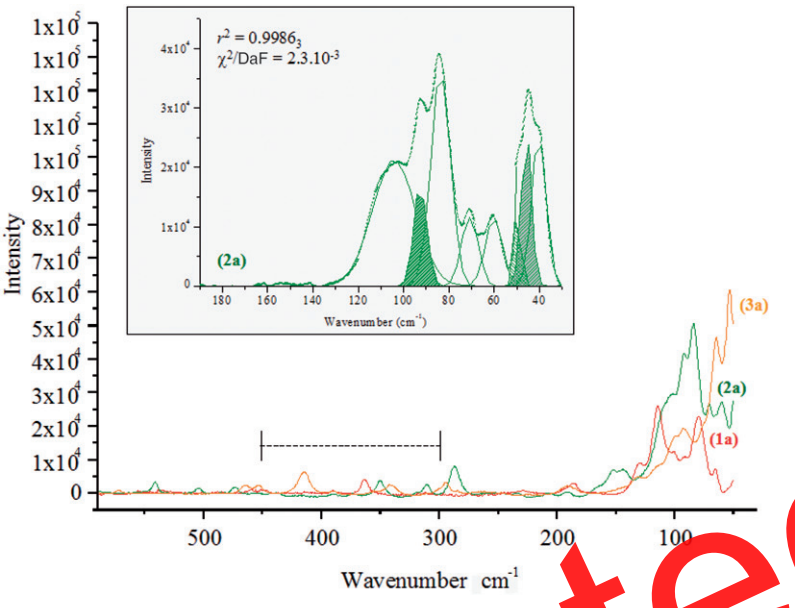

Figure 6. Solid-state Raman spectra of the Ag^{I}-, Zn^{II}-, and Cu^{II}-complexes of glycyl homohexapeptides (**1a**)–(**3a**) from 500 to 30 cm^{-1}. Small figure: Mathematical procedure for solid-state Raman spectrum of **2a** with baseline correction method and non-linear curve-fitting using the Gaussian to Lorenzian mixed function; The r^2 is (^{2}/DaF) statistical value.

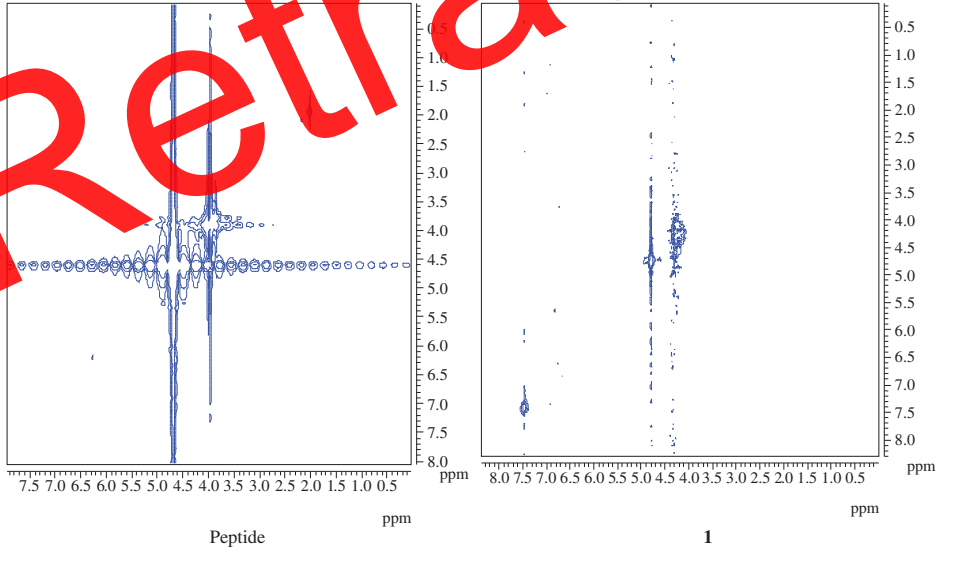

Figure 7. 2-D proton NMR data of cyclic pentapeptide and **1** in the solution of CD_3OD.

attributed to the $N_{(termini)}$, which participates in linkage and thus resonates at higher field than normal amides, which are observed at 7.1 and 7.2 ppm (figure 7). The CH_2 proton signals between 3.7 and 4.1 ppm of the free cyclic peptides was very complicated, indicating that the two protons are non-equivalent (figure 7). This indicates that the

Table 4. Theoretical Gibbs free energies (ΔG) (kcal mol^{-1}) according the PCM model using the B3LYP, or B3PW91 and M06-2X functionals at LANL2DZ, SDD, aug-cc-pVDZ or aug-cc-pVTZ basis sets (experimental).

1	−214.3	**2**	−243.7	**3***	−263.5	*H-(Gly)$_5$-OH*	−72.5	*c(Gly)$_3$*	−25.4	*c(Gly)$_3$-H*	−85.27
1a	−228.5	**2a**	−255.7	**3a***	−277.4	*H-(Gly)$_6$-OH*	−88.2	*c(Gly)$_4$*	−35.0	*c(Gly)$_4$-H*	−89.45
1b	−242.3	**2b**	−252.8	**3b**	−390.3	*H-(Gly)$_5$-COOH*	−96.9	*c(Gly)$_5$*	−38.5	*c(Gly)$_5$-H*	−85.0
1c	−319.2	**2c**	−272.1	**3c**	−398.4	*H-(Gly)$_6$-COOH*	−103.5	*c(Gly)$_6$*	−43.7	*c(Gly)$_6$-H*	−110.9
1d	−337.9			**3d**	−402.6						

*The *H-(Gly)$_n$-OH* and *H-(Gly)$_n$-COOH* ($n = 5$ or 6) are the corresponding zwitterion and protonated forms of the peptides; the *c(Gly)$_n$* and *c(Gly)$_n$-H*, where $n = 3$–6, are the cyclic derivatives, respectively.

peptides adopt an organized structure, in accord to the theoretical data [16]. Assignment of the glycyl-residues summarized in table 4 was performed using the R, S notation [16e, f]. The signals of the R-proton shift to higher field than those of the S-protons. The corresponding vicinal coupling constants agree reasonably well with the literature data [16] and conformational analysis indicates *cis–trans* isomerism of the cyclic derivatives, affecting the resonances of each residue of these peptides (scheme 1). Interpretation of the coordination of the metal ions by nuclear magnetic resonance data for the cyclic peptides was achieved taking into account the possibility for different conformations of the peptides in the metal complexes and existence of more than one stable conformer in solution. Sterically allowed molecular conformations in cyclic peptides are greatly reduced by ring closure. Since two sets of resonances were found in NMR spectra of the complexes of cyclic peptides (figure 7), two different molecular conformations simultaneously present in the solutions were assumed. The small $\Delta\delta$ of the *CH$_2$*-signals of one of the sets, compared to free ligands resulted in assignment to non-reacted peptides, in accord to the mass spectrometric data (above). The proton chemical shift of the peptide signals in complexes of Ag^{I} were within 0.5–1.5 ppm, in contrast to the corresponding Zn^{II}-complexes, where a smaller chemical shift of the signals ($\Delta\delta = 0.3$–0.9 ppm) was found (table 5). Coordination to metal ions affects the vicinal coupling constants, more significantly in the corresponding Ag^{I}-complexes. Coordination through oxygen of O=C was confirmed by the obtained chemical shifts from the ^{13}C-NMR data (table 5, scheme 2).

3.6. *Theoretical analysis*

The most stable conformers of the cyclic peptides and their protonated forms are summarized in table 4 (scheme 1). Since the obtained q_N(NBO) values for all of the amine nitrogen atoms are within the range of (−0.645) to (−0.667), the corresponding protonated forms are calculated according to the lowest values (scheme 1). In all cases the stable NH···O=C intramolecular hydrogen bond defines the most stable conformer (2.567–2.791 Å). ΔG values of the neutral cyclic peptides increased with increasing size of the rings. For the protonated forms, however, within the tripeptide to pentapeptide, the tetrapeptide shows higher ΔG of (−85.27) to (−89.45) kcal mol^{-1}. The protonated cyclichexapeptide shows significant stability since $\Delta G = -110.99$ kcal mol^{-1}. These data could be associated with the increasing number of hydrogen bonds in the cyclic molecules causing redistribution of the partial charges of the polar functional groups within the amide chains. The most stable complex is found to be the protonated

Table 5. ^{1}H and ^{13}C-NMR chemical shifts (in CD_3OD), δ [ppm] and J [Hz] of the cyclic penta and hexapeptides and their Ag^{I}- and Zn^{II}-complexes.

^{1}H-NMR

	Cyclic-pentapeptide				**1**				**2**			
	H_S	H_R	$^{3}J_{(NH-CHR)}$	$^{2}J_{(CHS-CHR)}$	H_S	H_R	$^{3}J_{(NH-CHR)}$	$^{2}J_{(CHS-CHR)}$	H_S	H_R	$^{3}J_{(NH-CHR)}$	$^{2}J_{(CHS-CHR)}$
gly_1-CH_2	3.89	3.38	3.82	−17.30	4.36	4.62	5.32	−18.20	4.17	3.88	4.08	−18.21
gly_2-CH_2	3.45	3.25	4.05	−16.13	4.21	4.03	5.17	−16.72	3.90	3.92	4.15	−17.05
gly_3-CH_2	3.78	3.80	5.81	−17.22	3.90	3.99	4.59	−17.92	3.69	4.08	4.24	−17.82
gly_4-CH_2	4.04	4.00	4.92	−15.88	4.57	4.18	5.02	−16.28	4.23	4.10	5.02	−16.38
gly_5-CH_2	4.06	4.05	4.58	−18.41	4.10	4.21	5.82	−19.53	4.12	4.15	4.70	−19.26
	Cyclic-hexapeptide				**1a**				**2a**			
	H_S	H_R	$^{3}J_{(NH-CHR)}$	$^{2}J_{(CHS-CHR)}$	H_S	H_R	$^{3}J_{(NH-CHR)}$	$^{2}J_{(CHS-CHR)}$	H_S	H_R	$^{3}J_{(NH-CHR)}$	$^{2}J_{(CHS-CHR)}$
gly_1-CH_2	3.78	3.42	3.96	−18.27	5.22	4.98	5.97	−20.19	4.22	3.93	4.88	−20.28
gly_2-CH_2	3.50	3.27	4.17	−15.34	4.37	4.14	5.89	−18.34	3.98	3.99	4.96	−21.72
gly_3-CH_2	3.80	3.88	5.92	−16.29	4.03	4.06	4.94	−19.76	3.94	4.21	4.90	−19.73
gly_4-CH_2	4.13	4.05	4.77	−17.11	4.66	4.33	5.16	−15.19	4.50	4.40	6.22	−19.49
gly_5-CH_2	4.21	4.11	4.41	−19.25	4.26	4.50	5.25	−20.17	4.37	4.56	4.62	−19.10
gly_6-CH_2	3.97	3.69	4.07	−18.29	4.05	3.90	4.82	−20.03	4.03	4.00	3.86	−17.54

^{13}C-NMR

	Cyclic-pentapeptide	**1**	**2**	Cyclic-hexapeptide	**1a**	**2a**
gly_1-CO	175.6	180.3	178.2	175.3	181.9	180.2
gly_1-CH_2	45.8	46.2	46.0	45.9	46.8	46.7
gly_2-CO	173.8	177.2	175.0	173.0	178.3	176.2
gly_2-CH_2	45.9	46.5	45.9	45.5	49.2	46.6
gly_3-CO	172.6	179.1	176.3	171.9	180.7	177.2
gly_3-CH_2	46.4	46.8	46.3	46.2	47.2	47.1
gly_4-CO	171.8	175.7	174.2	171.5	176.3	175.1
gly_4-CH_2	46.7	46.9	45.8	46.8	47.7	46.9
gly_5-CO	171.2	172.3	171.7	171.1	173.1	172.5
gly_5-CH_2	46.9	47.3	47.1	47.0	47.9	48.0
gly_6-CO				171.0	171.1	171.5
gly_6-CH_2				47.3	47.5	47.3

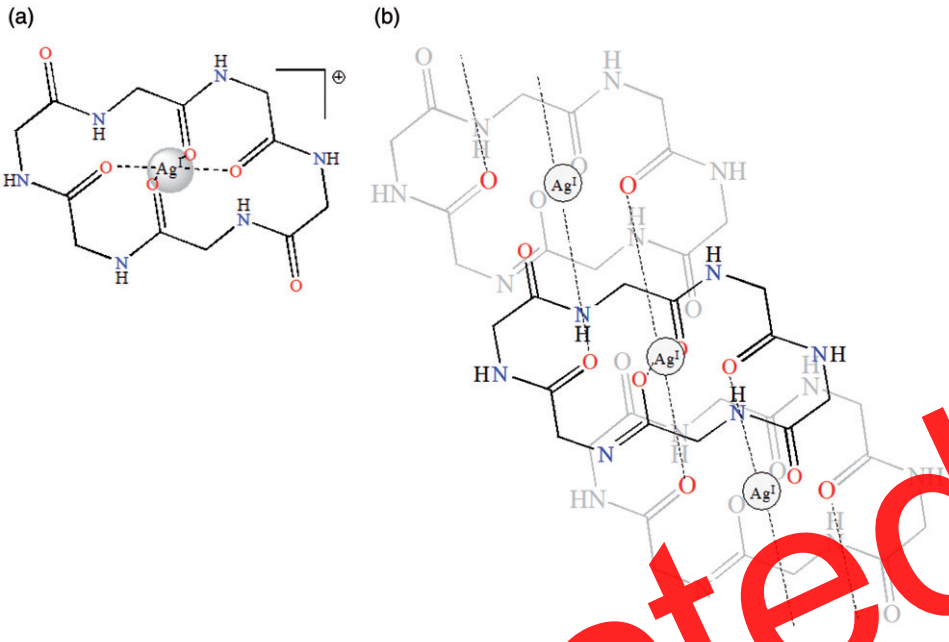

Scheme 2. Proposed gas-phase stabilized complex of Ag^I with *cyclo*-$(Gly)_5$-*H* (a) and its obtained derivative in solid-state (b), fitted best to the crystallographic data shown in figure 2.

divalent metal complexes, observed experimentally by mass spectrometric intensity of corresponding peaks for the metal species (figures 1 and 3, table 4). The complexes with the cyclic peptides have been optimized structurally using one metal ion. In contrast to the naturally obtained Ag^I-analogous [1a–c], where four silver ions are sandwiched between two cyclic peptide ligands, our calculations for the small ring systems showed that in the presence of two metal ions a significant repulsion results in increasing ΔG. In the free ligands each nitrogen points toward the center of the flat planar amide fragments in the macrocycle. In the corresponding natural analogues total planarity of the amide fragments in the macrocycle has been found by single-crystal X-ray diffraction for **1** [1a–c]. Upon complexation with Ag^I, however, the macrocycle turns inside out and the carbonyl groups all point toward the center of the macrocycle with the oxazoline rings orientated almost orthogonal to the macrocycle (schemes 1 and 2).

4. Conclusions and outlook

We highlight the coordination ability of linear and cyclic peptides with Ag^I, Zn^{II}, and Cu^{II}, respectively. Depending on the experimental conditions Ag^I/Ag^{III} redox is observed at pH 7.4–9.2, leading to the formation of corresponding Ag^{III}-complexes with the peptides. In all 14 species MLCT plays an important role, both in gas as well as in condensed phase, where the corresponding optical properties are elucidated [4f–i]. The observed optical and gas-phase phenomena are elucidated by electronic absorption and vibrational (IR- and Raman) spectroscopies within the *mid*- and *far*-IR region,

ESI-MS/MS, and MALDI-MSI Orbitrap methods. The 3-D conformations and the structures of peptides and their complexes are discussed using DFT calculations. In contrast to the corresponding linear peptides where tetradentate coordination through $N_{(termini)}$ of the ligand and deprotonation of the amide are observed, the cyclic derivatives show macrocyclic crown-ether coordination through the O-amide centers. The molar ratio 1 : 1 was found for the complexes, where the cyclic peptides are polydentate through (C=O) amide fragments. The molecular structure of Ag^{I}-cyclic pentapeptide was determined theoretically and experimentally in the triclinic space system and space group $P\bar{1}$. $Ag^{I}O_4$ has a distorted T_d symmetry as a result of molecule stretching in the complex (2.521(3)–2.569(4) Å). An additional weak Π-interaction with an amide gly_5 (resp. gly_5 and gly_6) C=O was found by proton shift in the corresponding mass spectra. By the combination of spectroscopic techniques, the complexes in solution were characterized with the different molecular conformations of free ligands and complexes in the solid-state, as found in a series of complexes obtained using the corresponding cyclic natural peptides [1a–e, 8a–f]. It has been proposed that metals could be involved in biological assembly of cyclic peptides, and cyclic peptide–metal conjugates probably evolved to carry out specific biological functions. Clearly, there are interdisciplinary aspects of the biology and ecological functions of such ligands that await further exploration. The presented results illustrate the capability of MALDI-MSI for elucidation, both qualitatively and quantitatively, of metal coordination with the cyclic peptides as relatively small molecular systems allowing their imaging in related biological systems.

Acknowledgments

The authors thank the Deutscher Akademischer Austausch Dienst (DAAD) for a grant within the priority program "Stability Pact South-Eastern Europe" and thank the Deutsche Forschungsgemeinschaft (DFG) for Grants SPP 255/21-1 and SPP/22-1. The authors also thank the central instrumental laboratories for structural analysis at Technological University Dortmund (TUD, Germany) and the analytical and computational laboratories at the Institute of Environmental Research (INFU) at the TUD.

References

[1] (a) A. Bertram, G. Pattenden. *Nat. Prod. Rep.*, **24**, 18 (2007); (b) P.Wipf, S. Venkatraman, C.P. Miller, S. Geib. *Angew. Chem., Int. Ed.*, **33**, 1516 (1994); (c) P. Wipf, C. Miller, C. Grant. *Tetrahedron*, **56**, 9143 (2000); (d) J. Davies. In *Cyclic Polymers*, J. Semlyen, E. Anthony (Eds), 2nd Edn, Kluwer Academic Publishers, Dordrecht, The Netherlands (2000); (e) D. Faulkner. *Nat. Prod. Rep.*, **5**, 613 (1988); (f) M. Rosen, S. Schreiber. *Angew. Chem. Int. Ed.*, **31**, 384 (1992); (g) D. Storm, K. Rosenthal, P. Swanson. *Annu. Rev. Biochem.*, **46**, 723 (1977); (h) F. Kondo, H. Matsumoto, S. Yamada, N. Ishikawa, E. Ito, S. Nagata, Y. Ueno, M. Suzuki. *Chem. Res. Toxicol.*, **9**, 1355 (1996); (i) T. Satoh, J. Arami, S. Li, T. Friedman, J. Gao, A. Edling, R. Townsend, U. Koch, S. Chocksi, M. Germann, R. Korngold, Z. Huang. *J. Biol. Chem.*, **272**, 12175 (1997); (j) W. Duax, J. Griffin, D. Langs, G. Smith, P. Grouchulski, V. Pletnev, V. Ivanov. *Biopolymers (Peptide Sci.)*, **40**, 141 (1996); (k) M. Ihara, M. Ishikawa, T. Fukuroda, T. Saeki, K. Funabashi, T. Fukami, H. Suda, M. Yano. *J. Cardiovasc.*

Pharmacol., **20**, S11 (1992); (l) A. Yiotakis, A. Lecoq, S. Vassiliou, I. Raynal, P. Cuniasse, V. Dive. *J. Med. Chem*., **37**, 2713 (1994).

[2] (a) N. Fusetani, T. Sugawara, S. Matsunaga, H. Hirota, A. Orbiculamide. *J. Am. Chem. Soc*., **113**, 7811 (1991); (b) D. Fairlie, G. Abbenante, D. March. *Curr. Med. Chem*., **2,** 654 (1995); (c) H. Breithaupt. *Nature Biotech*., **17**, 1165 (1999); (d) R. Kohil, C. Walsh, M. Burkart. *Nature*, **418**, 658 (2002); (e) M. Van Dyke, H. Lee, J. Trevors. *Biotechnol. Adv*., **9**, 241 (1991).

[3] (a) A. Jonsson. *Cell. Mol. Life Sci*., **58,** 868 (2001); (b) J. Yates. *J. Mass Spectrom*., **33**, 1 (1998); (c) I. Papayannopoulos. *Mass Spectrom. Rev*., **14**, 49 (1995); (d) K. Skold, M. Svensson, A. Kaplan, L. Bjorkesten, J. Astrom, P. Andren. *Proteomics*, **2**, 447 (2002); (e) R. Johnson. In *Proteome Research: Mass Spectrometry*, P. James (Ed.), Spinger-Verlag, Berlin, Germany (2001); (f) D. Cornett, M. Reyzer, P. Chaurand, R. Caprioli. *Nat. Methods*, **4**, 828v (2007); (g) T. Sinha, S. Khatib-Shahidi, T. Yankeelov, K. Mapara, M. Ehtesham, D. Cornett, B. Dawant, R. Caprioli, J. Gore. *Nat. Methods*, **5**, 57 (2008); (h) M. Glinski, W. Weckwerth. *Mass Spectrom. Rev*., **25**, 173 (2006); (i) M. Claydon, S. Davey, V. Jones, D. Gordon. *Nat. Biotechn*., **14**, 1584 (1996); (j) M. Pacholski, N. Winograd. *Chem. Rev*., **99**, 2977 (1999); (k) Y. Li, B. Shrestha, A. Vertes. *Anal. Chem*., **80**, 407 (2008); (l) K. Burnum, S. Frappier, R. Caprioli. *Annu. Rev. Anal. Chem*., **1**, 689 (2008); (m) R. Cole (Ed.). *Electrospray and MALDI Mass Spectrometry*, Wiley, New York (2010); (n) H. Lisa, D. Cazares, A. Dean, B. Wang, R. Richard, O. Semmes. *Anal. Bioanal. Chem*., **401**, 17 (2011); (o) A. Römpp, S. Guenther, Z. Takats, B. Spengler. *Anal. Bioanal. Chem*., **401**, 65 (2011); (p) H. Erin, R. Caprioli. *Trends Biotechnol*., **29**, 136 (2011); (q) E. Esquenazi, Y. Yang, J. Watrous, W. Gerwickac, P. Dorrestein. *Nat. Prod. Rep*., **26**, 1521 (2009).

[4] (a) J. Charalambous. *Mass Spectrometry of Metal Compounds*, Butterworths, London (1975); (b) M. Williams, J. Brodbelt. *J. Am. Soc. Mass. Spectrom*., **15**, 1039 (2004); (c) W. Henderson, B. Nicholson, L. McCaffrey. *Polyhedron*, **17**, 4291 (1998); (d) M. Litzow, T. Spalding. *Mass Spectrometry of Inorganic and Organometallic Compounds*, Elsevier, Amsterdam (1973); (e) M. Dale, P. Dyson, P. Suman, R. Zenobi. *Organometallics*, **16**, 197 (1996); (f) M. Dale, P. Dyson, B. Johnson, T. Langridge-Smith, H. Yates. *Dalton Trans*., 771 (1996).

[5] (a) M. Teyssot, A. Jarrousse, M. Manin, A. Chevry, S. Roche, E. Norre, C. Beaudoin, L. Morel, D. Boyer, R. Mahiou, A. Gautier. *Dalton Trans*., **35**, 6894 (2009); (b) B. Thati, A. Noble, B. Creaven, M. Walsh, M. McCann, K. Kavanagh, M. Devereux, D. Egan. *Cancer Lett*., **248**, 321 (2007); (c) H. Zhu, X. Zhang, X. Liu, X. Wang, G. Liu, H. Jun. *Inorg. Chem. Commun*., **6**, 1113 (2003); (d) J. Liu, P. Galettis, A. Farr, L. Maharaj, H. Samarasinha, A. McGechan, P. Baguley, R. Bowen, S. Berners-Price, M. McKeage. *J. Inorg. Biochem*., **102**, 303 (2008); (e) D. Medvetz, K. Hindi, M. Panzner, A. Ditto, H. Yun, W. Youngs. *Met. Based Drugs*, **2008**, 384010 (2008); (f) S. Patil, J. Claffey, A. Deally, M. Hogan, B. Gleeson, L. Méndez, H. Müller-Bunz, F. Paradisi, M. Tacke. *Eur. J. Inorg. Chem*., 1020 (2010); (g) T. Siciliano, M. Deblock, H. Hindi, S. Durmus, M. Panzner, C. Tessier, W. Youngs. *J. Organomet. Chem*., **696**, 1066 (2011); (h) S. Ray, R. Mohan, J. Singh, M. Samantaray, M. Shaikh, D. Panda, P. Ghosh. *J. Am. Chem. Soc*., **129**, 15042 (2007); (i) M. Sriram, S. Kanth, K. Kalishwaralal, S. Gurunathan. *Intern. J. Nanomedicine* **5**, 753 (2010); (j) J. Kim, E. Kuk, K. Yu. *Nanomedicine*, **3**, 95 (2007); (k) C. Baker, A. Pradhan, L. Pakstis. *J. Nanosci. Nanotechnol*., **5**, 244 (2005).

[6] (a) M. Awouafack, P. Spiteller, M. Lamshöft, S. Kusari, B. Ivanova, P. Tane, M. Spiteller. *J. Nat. Prod*., **74**, 272 (2011); (b) M. Awouafack, S. Kusari, M. Lamshöft, D. Ngamga, P. Tane, M. Spiteller. *Planta Medica*, **76**, 640 (2010); (c) S. Kusari, S. Zühlke, M. Spiteller. *Phytochem. Anal*., **22**, 128 (2010); (d) S. Kusari, S. Zühlke, T. Borsch, M. Spiteller. *Phytochem*., **70**, 1222 (2009); (e) S. Kusari, S. Zühlke, M. Spiteller. *J. Nat. Prod*., **74**, 764 (2011); (f) S. Kusari, S. Zühlke, M. Spiteller. *J. Nat. Prod*., **72**, 2 (2009); (g) S. Kusari, S. Zühlke, J. Košuth, E. Cellárová, M. Spiteller. *J. Nat. Prod*., **72**, 1825 (2009); (h) S. Kusari, M. Lamshöft, S. Zühlke, M. Spiteller. *J. Nat. Prod*., **71**, 159 (2008); (i) S. Kusari, M. Spiteller. *Nat. Prod. Rep*., **28**, 1203 (2011); (j) S. Puri, V. Verma, T. Amna, C. Qazi, M. Spiteller. *J. Nat. Prod*., **68**, 1717 (2005); (k) B. Kindler, H. Kraemer, S. Nies, P. Gradicsky, G. Haase, P. Mayser, M. Spiteller, P. Spiteller. *Eur. J. Org. Chem*., **11**, 2084 (2010); (l) J. Reetz, S. Zühlke, M. Spiteller, K. Wallner. *Apogologie*, **42**, 596 (2011).

[7] (a) T. Kolev, B. Koleva, S. Zareva, M. Spiteller. *Inorg. Chim. Acta*, **359**, 4367 (2007); (b) B. Koleva, T. Kolev, M. Spiteller. *Inorg. Chim. Acta*, **360**, 2224 (2007); (c) B. Koleva, S. Zareva, T. Kolev, M. Spiteller. *J. Coord. Chem*., **61**, 3534 (2008); (d) B. Koleva, T. Kolev, M. Lamshöft, M. Spiteller. *Trans. Met. Chem*., **33**, 911 (2008); (e) T. Kolev, B. Koleva, M. Spiteller. *J. Coord. Chem*., **61**, 1897 (2008); (f) B. Ivanova, M. Spiteller. *Polyhedron*, **30**, 241 (2011); (g) M. Lamshöft, J. Storp, B. Ivanova, M. Spiteller. *Polyhedron*, **30**, 2564 (2011); (h) M. Lamshoeft, B. Ivanova. *J. Coord. Chem*., **64**, 2419 (2011); (i) S. Cho, M. Mara, X. Wang, J. Lockard, A. Rachford, F. Castellano, L. Chen. *J. Phys. Chem. A*, **115**, 3990 (2011); (j) M. Lamshöft, J. Storp, B. Ivanova, M. Spiteller. *Inorg. Chim. Acta*, **382**, 96 (2012).

[8] (a) M. Gross, D. McCrery, F. Crow, K. Tomer, M. Pope, L. Cuifetti, H. Knoch, J. Daly, L. Dunkle. *Tetrahedron Lett*., **23**, 5381 (1982); (b) K. Tomer, F. Crow, M. Gross. *Anal. Chem*., **56**, 880 (1984); (c) K. Eckart, H. Schwarz, K. Tomer, M. Gross. *J. Am. Chem. Soc*., **107**, 6765 (1985); (d) K. Eckart. *Mass Spectrom. Rev*., **13**, 23 (1994); (e) L. Ngoka, M. Gross, P. Toogood. *Int. J. Mass Spectrom*., **182/183**, 289 (1999); (f) C. Lambert, L. Ngoka, M. Gross. *J. Am. Soc. Mass. Spectrom*., **10**, 732 (1999);

(g) G. Spiteller. *Massspektrometrishe Strukturanalyse organisher Verbindungen*, Verlag Chemie, Weinbeim (1966); (h) J. Gilpin. *Anal. Chem.*, **31**, 935 (1959); (i) Z. Pelah, M. Kielczewski, J. Wilson, M. Ohashi, H. Budzikiewicz, C. Djerassi. *J. Am. Chem. Soc.*, **85**, 2470 (1963); (j) C. Fernandes, R. Moreira, L. Lube, A. Horn Jr., B. Szpoganicz, S. Sherrod, D. Russell. *Dalton Trans.*, **39**, 5094 (2010).

[9] (a) G.M. Sheldrick. *Acta Cryst.*, **A64**, 112 (2008); (b) G.M. Sheldrick. *Acta Cryst.*, **D66**, 479 (2010); (c) G.M. Sheldrick. *Acta Cryst.*, **A46**, 467 (1990); (d) R. Blessing. *Acta Cryst.*, **A51**, 33 (1995); (e) A. Spek. *J. Appl. Cryst.*, **36**, 7 (2003).

[10] (a) M. Frisch, G. Trucks, H. Schlegel, G. Scuseria, M. Robb, J. Cheeseman, V. Zakrzewski, J. Montgomery Jr., R. Stratmann, J. Burant, S. Dapprich, J. Millam, A. Daniels, K.N. Kudin, M. Strain, O. Farkas, J. Tomasi, V. Barone, M. Cossi, R. Cammi, B. Mennucci, C. Pomelli, C. Adamo, S. Clifford, J. Ochterski, G.A. Petersson, P. Ayala, Q. Cui, K. Morokuma, D. Malick, A. Rabuck, K. Raghavachari, J. Foresman, J. Cioslowski, J. Ortiz, B. Stefanov, G. Liu, A. Liashenko, P. Piskorz, I. Komaromi, R. Gomperts, R. Martin, D. Fox, T. Keith, M. Al-Laham, C. Peng, A. Nanayakkara, C. Gonzalez, M. Challacombe, P. Gill, B. Johnson, W. Chen, M. Wong, J. Andres, C. Gonzalez, M. Head-Gordon, E. Replogle, J. Pople. *Gaussian 98, Revision A.3*, Gaussian Inc., Pittsburgh, PA (1998); M. Frisch, G. Trucks, H. Schlegel, G. Scuseria, M. Robb, J. Cheeseman, G. Scalmani, V. Barone, B. Mennucci, G. Petersson, H. Nakatsuji, M. Caricato, X. Li, H. Hratchian, A. Izmaylov, J. Bloino, G. Zheng, J. Sonnenberg, M. Hada, M. Ehara, K. Toyota, R. Fukuda, J. Hasegawa, M. Ishida, T. Nakajima, Y. Honda, O. Kitao, H. Nakai, T. Vreven, J. Montgomery, Jr., J. Peralta, F. Ogliaro, M. Bearpark, J. Heyd, E. Brothers, K. Kudin, V. Staroverov, R. Kobayashi, J. Normand, K. Raghavachari, A. Rendell, J. Burant, S.S. Iyengar, J. Tomasi, M. Cossi, N. Rega, J. M. Millam, M. Klene, J. E. Knox, J.B. Cross, V. Bakken, C. Adamo, J. Jaramillo, R. Gomperts, R. Stratmann, O. Yazyev, A. Austin, R. Cammi, C. Pomelli, J. Ochterski, R. Martin, K. Morokuma, V. Zakrzewski, G. Voth, P. Salvador, J. Dannenberg, S. Dapprich, A. Daniels, O. Farkas, J. Foresman, J. Ortiz, J. Cioslowski, D. Fox. *Gaussian 09W, Revision A.1*, Gaussian, Inc., Wallingford, CT (2009); (b) Dalton 2.0 Program Package. Available online at: http://dirac.chem.sdu.dk/daltonprogram.org/ (accessed 28 March 2012); (c) GausView03. Available online at: http://www.cyberchem.com/gaussview.htm (accessed 28 March 2012); (d) P. Politzer. In *Chemical Applications of Atomic and Molecular Potentials*, P. Politzer, D. Truhlar (Eds), Plenum Press, New York (1981); (e) Y. Zhao, D. Truhlar. *Accts. Chem. Res.*, **41**, 157 (2008); (f) N. Schultz, Y. Zhao, D. Truhlar. *J. Comput. Chem.*, **29**, 185 (2008); (g) Y. Zhao, D. Truhlar. *Theor. Chem. Acc.*, **120**, 215 (2008); (h) D. Woon, T. Dunning. *J. Chem. Phys.*, **98**, 1358 (1993); (i) G. Olah, S. Kuhn, J. Flood. *J. Am. Chem. Soc.*, **84**, 1688 (1962); (j) G. Olah, S. Kuhn, J. Flood. *J. Am. Chem. Soc.*, **84**, 1695 (1962); (k) E. Wilson. *J. Chem. Phys.*, **36**, 2232 (1962); (l) F. Jensen. *Introduction to Computational Chemistry*, Wiley, New York (1999); (m) M. Head-Gordon, J. Pople, M. Frisch. *Chem. Phys. Lett.*, **153**, 503 (1988); (n) W. Hehre, L. Radom, P. Schleyer, J. Pople. *Ab Initio Molecular Orbital Theory*, Wiley, New York (1986); (o) J. Autschbach, F. Jorge, T. Ziegler. *Inorg. Chem.*, **42**, 2867 (2002); (p) J. Cooper, T. Ziegler. *Inorg. Chem.*, **41**, 6614 (2002); (q) F. Jorge, J. Autschbach, T. Ziegler. *Inorg. Chem.*, **42**, 8902 (2003); (r) K. Wiberg, C. Hadad, J. Foresman, W. Chupka. *J. Phys. Chem.*, **96**, 10756 (1992); (s) T. Truong, E. Stefanovich. *Chem. Phys. Lett.*, **240**, 253 (1995); (t) B. Ivanova, M. Spiteller. *Biopolymers*, **39**, 727 (2010); (u) B. Ivanova, M. Spiteller. *Biopolymers*, **97**, 134 (2011); (v) B. Ivanova, M. Spiteller. *J. Mol. Struct.*, **1004**, 303 (2011); (w) B. Ivanova, M. Spiteller. *J. Mol. Struct.*, **1003**, 1 (2011); (x) B. Ivanova, M. Spiteller. *J. Pharmaceut. Biomed. Anal.*, DOI: 10.1016/j.jpba.2011.10.028 (2011); (y) B. Ivanova, M. Spiteller. *Talanta* (2011), in press.

[11] (a) Available online at: http://de.openoffice.org/ (accessed 28 March 2012); (b) C. Kelley. *Iterative Methods for Optimization*, *SIAM Frontiers in Applied Mathematics*, Vol. 18, SIAM, Philadelphia (1999); (c) K. Madsen, H. Nielsen, O. Tingleff. *Informatics and Mathematical Modelling*, 2nd Edn, DTU Press, Lyngby (2004); (d) P. Stephens, D. McCann, J. Cheeseman, M. Frisch. *Chirality*, **17**, S52 (2005); (e) P. Stephens, F. Devlin, J. Cheeseman, M. Frisch, O. Bortolini, P. Besse. *Chirality*, **15**, S57 (2003); (f) A. Yildiz, P. Selvin. *Accts. Chem. Res.*, **38**, 574 (2005); (g) M. Lamshöft, B. Ivanova, M. Spiteller. *Talanta*, **85**, 2562 (2011).

[12] (a) H. Schwalbe, J. Wermuth, C. Richter, S. Szalma, A. Eschenmoser, G. Quinkert. *Helv. Chim. Acta*, **83**, 1079 (2000); (b) C. Beguin, S. Hamman. *Org. Mag. Res.*, **16**, 129 (1981); (c) J. McDonald. *Can. J. Mag. Res.*, **34**, 207 (1979); (d) M. Kainosho, K. Ajisaka. *J. Am. Chem. Soc.*, **97**, 5630 (1975); (e) J. Feeney, P. Hansen, C. Roberts. *Chem. Commun.*, 465 (1974); (f) A. Piccolo, M. Spiteller. *Anal. Bioanal. Chem.*, **377**, 1047 (2003); (g) C. McIntyre, B. Batts, D. Jardine. *J. Mass. Spectrom.*, **32**, 328 (1997); (h) U. Klaus, T. Pfeifer, M. Spiteller. *Environ. Sci. Technol.*, **34**, 3514 (2000); (i) T. Pfeifer, K. Uwe, R. Hoffmann, M. Spiteller. *J. Chrom.*, **926**, 151 (2001); (j) E. Cole. *J. Mass Spectrom.*, **35**, 763 (2000); (k) L. Brown, J.A. Rice. *Anal. Chem.*, **72**, 384 (2000).

[13] (a) B. Ganem, Y.-T. Li, J.D. Henion. *J. Am. Chem. Soc.*, **113**, 7818 (1991); (b) M. Moniatte, C. Lesieur, B. Vecsey-Semjen, J. Buckley, F. Pattus, F. van der Goot, F. Van Dorsselaer. *J. Am. Soc. Mass Spectrom.*, **8**, 1046 (1997); (c) S. Clark, L. Konermann. *J. Am. Soc. Mass Spectrom.*, **14**, 430 (2003); (d) S. Clark, D. Leaist, L. Konermann. *Rapid Commun. Mass Spectrom.*, **16**, 1454 (2002); (e) S. Clark, L. Konermann. *Anal. Chem.*, **76**, 1257 (2004).

[14] (a) R. Österberg, B. Sjöberg. *J. Biolog. Chem.*, **243**, 3038 (1968); (b) W. Beck. Z. Naturforschung B, **64**, 1221 (2009); (c) S. Rajković, M. Ivković, C. Kállay, I. Sóvágó, M. Djuran. *Dalton Trans.*, 8370 (2009); (d) S. Barry, G. Rickard, M. Pushie, A. Rauk. *Can. J. Chem.*, **87**, 942 (2009); (e) A. Biswas, E. Hughes, B. Sharma, J. Wilson. *Acta Crystallogr.*, **24B**, 40 (2968); (f) R. Parthasarathy. *Acta Crystallogr.*, **25B**, 509 (1969); (g) R. Meulemans, P. Piret, M. van Meerssche. *Acta Crystallogr.*, **27**, 1187 (1971); (h) B. Strandberg, I. Lindqvist, R. Rosenstein. *Z. Kristallogr.*, **116**, 266 (1961); (i) A. McLean, G. Chandler. *J. Chem. Phys.*, **72**, 5639 (1980).

[15] (a) W. Griffith. *J. Chem. Soc.*, 3694 (1965). (b) R. Feltham, W. Fateley. *Spectrochim. Acta A*, **20**, 1081 (1964); (c) J. Durig, W. McAllister, J. Willias, E. Mercer. *Spectrochim. Acta A*, **22**, 1001 (1966); (d) W. Griffith. *J. Chem. Soc. A*, 899 (1966); (e) J. Durig, R. Layton, D. Sink, B. Mitchell. *Spectrochim. Acta A*, **21**, 1367 (1965); (f) D. Powell. *Chem. Ind.*, 314 (1956); (g) F. Cotton, N. Curtis, W. Robinson. *Inorg. Chem.*, **4**, 1696 (1965); (h) D. Powel, N. Sheppard. *Spectrochim. Acta A*, **17**, 68 (1961); (i) D. Adams. *Metal-Ligand and Related Vibrations*, Edward Arnold Publishers Ltd., London (1967); (j) K. Nakamoto. *Infrared and Raman Spectra of Inorganic and Coordination Compounds*, John Wiley and Sons, New York, Chichester, Brisbane, Toronto (1978).

[16] (a) B. Perly, N. Helbecque, A. Forchioni, M. Loucheux-Lefebre. *Biopolymers*, **22**, 1853 (1983); (b) C. Grathwohl, A. Tun-Kyi, A. Bundi, R. Schwyzer, K. Wüthrich. *Helv. Chim. Acta*, **58**, 415 (1975); (c) J. Meraldi, R. Schwyzer, A. Tun-Kyi, K. Wüthrich. *Helv. Chim. Acta*, **55**, 1962 (1972); (d) J. Laussac, R. Hharan, B. Sarkar. *Biochem. J.*, **209**, 533 (1983); (e) J. Modder, K. Vrieze, A. Spek, G. Challa, G. van Koten. *Inorg. Chem.*, **31**, 1238 (1992); (f) M. Kainosho, K. Ajisaka, M. Kamisaku, A. Murai. *Biochem. Biophys. Res. Commun.*, **64**, 425 (1975); (g) G. Boussard, M. Marraud, A. Aubry. *Biopolymers*, **18**, 1297 (1979).